ECS Journal of Solid State Science and Technology, **2** (12) P515-P523 (2013)
2162-8769/2013/2(12)/P515/9/$31.00 © The Electrochemical Society

Oxygen Plasma and Humidity Dependent Surface Analysis of Silicon, Silicon Dioxide and Glass for Direct Wafer Bonding

A. U. Alam, M. M. R. Howlader,*,z and M. J. Deen**

Department of Electrical and Computer Engineering, McMaster University, Hamilton, Ontario L8S 4K1, Canada

Surface and interface characteristics of substrates are critical for reliable wafer bonding. Understanding the elemental and compositional states of surfaces after various processing conditions is necessary when bonding dissimilar materials. Therefore, we investigated the elemental and compositional states of silicon (Si), silicon dioxide (SiO_2) and glass surfaces exposed to oxygen reactive ion etching (O_2 RIE) plasma followed by storage in controlled humidity and/or ambient atmospheric conditions to understand the chemical mechanisms in the direct wafer bonding. High-resolution X-ray Photoelectron Spectroscopy (XPS) spectra of O_2 RIE treated Si, SiO_2 and glass showed the presence of $Si(-O)_2$ resulting in highly reactive surfaces. A considerable shift in the binding energies of $Si(-O)_2$, $Si(-O)_4$ and $Si(-OH)_x$ were observed only in Si due to plasma oxidation of the surface. The humidity and ambient storage of plasma activated Si and SiO_2 increased $Si(-OH)_x$ due to enhanced sorption of hydroxyls. The amounts of $Si(-O)_2$ and $Si(-OH)_x$ of Si varied in different humidity storage conditions which are attributed to crystal-orientation dependent surface morphology and oxidation. The O_2 RIE plasma induced high surface reactivity and humidity induced $Si(-OH)_x$ can play an important role in the hydrophilic wafer bonding with low temperature heating.
 [DOI: 10.1149/2.007312jss]

Manuscript submitted September 10, 2013; revised manuscript received October 14, 2013. Published October 22, 2013.

Emerging nanoelectronics, micro-electromechanical systems (MEMS) and microfluidic devices[1–5] require the integration of different substrates such as silicon (Si),[6] silicon dioxide (SiO_2)[7] and glass.[8] Direct bonding of these materials onto a common substrate requires proper surface treatments[9–13] to maintain desirable mechanical, electrical and chemical properties. Plasma surface activation using oxygen reactive ion etching (O_2 RIE)[14] is one of the most attractive surface treatment methods which eliminates high temperature annealing in wafer bonding. The surface elemental and compositional state dependent hydrophilicity (OH groups)/ hydrophobicity (H groups) and other physical properties such as morphology of the O_2 RIE treated surfaces play an important role in hydrophilic wafer bonding of Si/Si, Si/SiO_2, Si/glass.[15–17] For example, hydrophilic wafers might contain a monolayer of water when stored at a RH (relative humidity) of 50%, attached via hydrogen bonding to the surface OH groups.[18] The hydrogen bonding between adsorbed water molecules on the two surfaces makes the Si—OH$\cdots$(H_2O)$\cdots$OH—Si in Si wafer bonding.[18] X-ray photoelectron spectroscopy (XPS) is a versatile technique to analyze the elemental compositions and chemicals states of materials surfaces.

Previous XPS studies of Si included investigations of binding energy shift in ambient-exposed Si due to different chemical groups,[19] oxygen radical plasma activated Si/Ge bonded interface,[20] oxide layer thickness in oxygen plasma activated surfaces,[21] oxidized Si with ion-implanted oxygen,[22] contaminants (C_{1s} peak) and oxides (O_{1s} peak) in hydrogen plasma treated polycrystalline Si,[23] and high oxygen-to-silicon ratio in oxygen plasma treated Si generated by electron cyclotron resonance.[24] Similarly, the XPS analysis of SiO_2 included investigations of compositional stability after plasma treatments and aging,[25] crystal orientation dependent chemical shift due to distribution electric dipole moment at the interface of ultra-thin silicon oxide,[26] and different oxidation states of Si^{0+}, Si^{1+}, Si^{2+}, Si^{3+} and Si^{4+} after plasma anodization and rapid thermal annealing of Si.[27] Also XPS studies of glass included investigations of O_{1s} spectra in sodium silicate glass that indicated an increase in the ratio of non-bonding oxygen due to increase of iron concentration,[28] the presence of Si-CH bond (different from the Si-O bond) in silane-treated microscope glass slide surfaces,[29] drifting of oxygen from the Pyrex glass toward Si in Si/Pyrex glass laser bonding that controlled the bond strength,[30,31] and the O_{1s} spectra of silica and soda lime glasses at room temperature and humidity (RH:64%) which revealed that the nanoindentation hardness was dependent on the ratio of cuprous (Cu^+) and cupric (Cu^{2+}) ions.[32]

The majority of XPS studies on wafers discussed in the previous paragraph focused on plasma processing parameters not directly related to the bonding and packaging of microelectronic, MEMS and microfluidic devices. A literature survey showed that the plasma power that critically impact in the formation of OH and H ranges from 10–300 W with the activation time of up to 300 s and chamber pressure of up to 100 Pa.[14,33,34] Recently, we have investigated the surface activated bonding of Si, SiO_2 and glass treated by O_2 RIE without elemental and compositional analysis.[10,35,36] In all the cases of bonding, the bonding strength has been of paramount concern, but not much is known about the chemical state of Si, SiO_2 and glass after their surface treatments. Also, bonding of such materials for mass production may go through different ambient and humidity conditions which may influence their bondability.[37] Thus, an analysis of the chemical states and elemental compositions of the treated surfaces (with short and long activation times) to identify the role of plasma, ambient and humidity storage on the surfaces is needed.

In this paper, we investigated the chemical state and elemental composition of the surfaces of Si, SiO_2 and glass that were treated by oxygen reactive ion etching (O_2 RIE) plasma and humidity/ambient to identify the role on their bondability. The plasma-activated surfaces were treated in 15°C and 98% relative humidity with or without ambient storage in a cleanroom. These treatments enabled us to study the role of the plasma and humidity on the hydrophilic wafer bonding of these substrates. Wide scan and narrow scan X-ray photoelectron spectroscopy (XPS) spectra of the treated surfaces were acquired. The surface properties were analyzed by examining their binding energy shift, full-width-half-maximum (FWHM), and the amount of the chemical components.

Materials and Methods

The chemical analysis was done for three types of materials: (i) one-side mirror polished p-type 2-inch Si(100) wafers of 450 μm thickness, (ii) 2-inch SiO_2-on-Si wafers with 50 nm thick thermal oxides and (iii) 2-inch Glass (Pyrex from Schott, US) wafers. The glass wafers may contain alkaline elements similar to standard Pyrex glass. The as-received Si surface may have native oxides of less than 5 nm thicknesses.[38] For each experiment (i.e., surface activation and storage), three identical samples were used. These samples were cut from same lot of the wafers into 10×10 mm^2 pieces using a diamond needle. The surfaces were activated with O_2 oxygen reactive ion etching (RIE) plasma. The RIE plasma was produced in a chamber background pressure of 10 Pa at 13.85 MHz radio frequency in Hybrid Plasma Bonder (HPB) from Bondtech Corporation.[39] Different plasma activation times were selected such as 60, 150, 300, 600 and

*Electrochemical Society Active Member.
**Electrochemical Society Fellow.
zE-mail: mrhowlader@ece.mcmaster.ca

Table I. Description of the materials, their surface activation and storage conditions with their corresponding acronyms.

Acronyms	Surface Activation	Storage Conditions	Materials
Si:O_2RIE	O_2 RIE plasma	No storage	Si
Si:O_2RIE+20RH	O_2 RIE plasma	20 days of storage in 98% RH and 15°C temperature	Si
Si:O_2RIE:20D+20RH	O_2 RIE plasma	20 days of storage in class 1000 cleanroom ambient and 20 days in 98% RH and 15°C temperature	Si
SiO_2:O_2RIE	O_2 RIE plasma	No storage	SiO_2
SiO_2:O_2RIE+20RH	O_2 RIE plasma	20 days of storage in 98% RH and 15°C temperature	SiO_2
SiO_2:O_2RIE+20D+20RH	O_2 RIE plasma	20 days of storage in class 1000 cleanroom ambient and 20 days in 98% RH and 15°C temperature	SiO_2
Glass:O_2RIE	O_2 RIE plasma	No storage	Glass

1200 s. The plasma power was 300 W and the pressure during plasma glow was 200 Pa.

The activated Si and SiO_2 wafers were then kept in humidity and/or ambient storage. Table I shows the details of different types of plasma activation and storage conditions with their acronyms that will be used later in this paper. During storage in the humidity chamber (from ESPEC), the temperature and the relative humidity (RH) were held constant at 15°C and 98% RH, respectively. JPS-9200 from JEOL was used to acquire X-ray photoelectron spectroscopy (XPS) spectra for chemical analysis of the as-received, plasma activated and humidity/ambient treated surfaces. The Magnesium X-ray source with 12 kV and 15 mA was used for acquiring wide-scan and narrow-scan spectra with binding energy resolution of 0.1 eV. Also, the Ar-ion etching (with 3 keV) was done with 0.08 Pa pressure. The XPS instrument was calibrated using an Au sample.

In addition to the surface chemical analysis of Si, SiO_2, and glass, we have further investigated the role of their surface roughness, contact angle and hardness on direct wafer bonding.[40] To focus the work and have a reasonable length of the manuscript, the surface chemical analysis is studied in detail in this paper.

Results

Silicon.— The chemical states of the Si surfaces treated with O_2 RIE plasma activation and/or different storage conditions are shown in Figure 1. Charge correction was done by shifting the position of the Si_{2p} peak binding energy at 99.0 eV, since there was no significant Carbon (C) peak.[25] The wide-scan XPS spectra of as-received Si (Figure 1a) showed peaks at 100, 150, 284 and 532 eV for Si_{2p}, Si_{2s}, C and O_{1s}, respectively.[19,41] The wide-scan spectra of plasma-activated Si showed additional peaks of fluorine at 688 eV and Cu_{LVV} at 600 eV. However, 40 s etching of the plasma-activated surfaces using Ar-ion removed the fluorine peaks. Strong peaks for Si_{2p} and Si_{2s} were observed. High-resolution XPS spectra of O_{1s} and Si_{2p} peaks are shown in Figure 1b–1d and 1e–1f, respectively for different storage conditions.

The dashed and solid lines in Figure 1 indicate the O_{1s} and Si_{2p} peaks. The peak positions shifted to the higher binding energies with increased activation times. The O_{1s} and Si_{2p} peaks were deconvolved using the mixed Gaussian/Lorentzian function to understand the nature of the embedded components of the chemical elements. The maximum value of the full-width-half-maximum (FWHM) of the deconvolved peaks was 1.0 eV. The deconvolved O_{1s} and Si_{2p} peaks for the as-received Si are shown as typical examples in Figure 2a and 2b, respectively.[42–44] The peaks in the deconvolved O_{1s} spectra (Figure 2a) are mainly composed of $Si(-O)_2$, $Si(-OH)_x$ and $Si(-O)_4$ (tetrahedral silicon oxide) that appeared at 531.9, 531.1 and 532.9 eV, respectively. On the other hand, the deconvolved Si_{2p} spectra (Figure 2b) are composed of three peaks - Si, $Si(-OH)_x$ and $Si(-O)_2$ that appeared at 99.0, 99.5 and 102.6 eV, respectively. For further clarification of the influence of plasma, humidity and ambient on the $Si(-O)_2$, $Si(-OH)_x$ and $Si(-O)_4$, succinct results are given in the following paragraphs.

Table II summarizes the energy shifts and changes of FWHM of the deconvolved components of O_{1s} and Si_{2p} for Si at different plasma treatment and storage conditions. No noticeable changes in the binding energy, FWHM and percentage amounts of $Si(-O)_2$, $Si(-OH)_x$ and $Si(-O)_4$ were identified for the three identical specimens in each experiment. In the case of Si:O_2RIE, all three component peaks of O_{1s} spectra (i.e., $Si(-OH)_x$, $Si(-O)_2$, $Si(-O)_4$) showed significant positive energy shift. Also, the $Si(-O)_2$ component peak of Si_{2p} spectra showed significant positive energy shift since the Si component of Si_{2p} spectra is considered as reference for charge correction. The increase of FWHM of all the components in O_{1s} and Si_{2p} spectra was also significant.

For Si:O_2RIE+20RH, only $Si(-OH)_x$ component of O_{1s} spectra showed significant positive binding energy shift. But the $Si(-O)_2$ and $Si(-OH)_x$ components of Si_{2p} spectra did not show any considerable positive binding energy shift. Also, the overall FWHM of all the components of O_{1s} and Si_{2p} spectra were not considerably changed. For Si:O_2RIE+20D+20RH, only $Si(-OH)_x$ component of O_{1s} spectra showed considerable positive binding energy shift. But the $Si(-O)_2$ and $Si(-OH)_x$ components of Si_{2p} spectra did not show any considerable positive binding energy shift. Also, the overall FWHM of all the components of O_{1s} and Si_{2p} spectra were not considerably changed.

We used the Ar beam etch to determine the effects of oxidation on binding energy for Si:O_2RIE, Si:O_2RIE+20RH and Si:O_2RIE+20D+20RH. The results are shown by the 'Ar-Ion Etch' curves in Figure 1. After ~40 s of Ar-ion etching (pressure 0.08 Pa), the surface oxide was removed, as indicated by the disappearance of the oxide peaks in Figure 1b, 1c and 1d. Also, the $Si(-O)_2$ peaks of Si_{2p} spectra in Figure 1e, 1f and 1g disappeared after Ar-ion etching. The Si peak had then moved to a lower binding energy, which indicates that oxidation increases binding energy.

We have also summarized the amount of $Si(-O)_2$, $Si(-OH)_x$ and $Si(-O)_4$ from the deconvolved O_{1s} and Si_{2p} spectra as a function of activation time with or without storage in ambient and humidity in Figure 3. Figure 3a-3c corresponds to Figure 1b–1d, respectively.

Silicon dioxide.— Figure 4a shows the wide-scan spectra of SiO_2:O_2RIE. Charge correction was done by shifting the position of the C peak binding energy at 284 eV. The peaks at 100, 150, 284, 531 933 and 953 eV are for Si_{2p}, Si_{2s}, C, O_{1s}, $Cu_{2p3/2}$, and $Cu_{2p1/2}$, respectively.[41] There was no significant difference between the wide scan spectra of plasma activated and Ar-ion etched SiO_2. Figure 4b shows the high-resolution O_{1s} and Si_{2p} spectra of SiO_2 surfaces treated with O_2 RIE plasma and different storage conditions. The dashed lines and the solid lines in the O_{1s} spectra (Figure 4b, 4c, 4d) indicate the $Si(-O)_4$ and $Si(-O)_2$ peaks, respectively. Similarly, the dashed lines and solid lines in the Si_{2p} spectra (Figure 4e, 4f, 4g) indicate the $Si(-O)_2$ and Si_0 peaks, respectively.

Although the $Si(-O)_2$ and Si_0 peaks in Si_{2p} spectra are easily distinguishable, there was a hidden peak of $Si(-OH)_x$ in between $Si(-O)_4$ and $Si(-O)_2$ peaks in O_{1s} spectra.[45] In order to quantify these three peaks at different plasma activation and storage conditions, the O_{1s} spectra were deconvolved using mixed Gaussian/Lorentzian function with maximum FWHM of 1 eV. Figure 5 shows a typically deconvolved O_{1s} spectra of as received SiO_2 consisting of $Si(-O)_2$, $Si(-OH)_x$ and $Si(-O)_4$.[45] They appeared at 530.4, 531.6 and 533.4 eV, respectively.

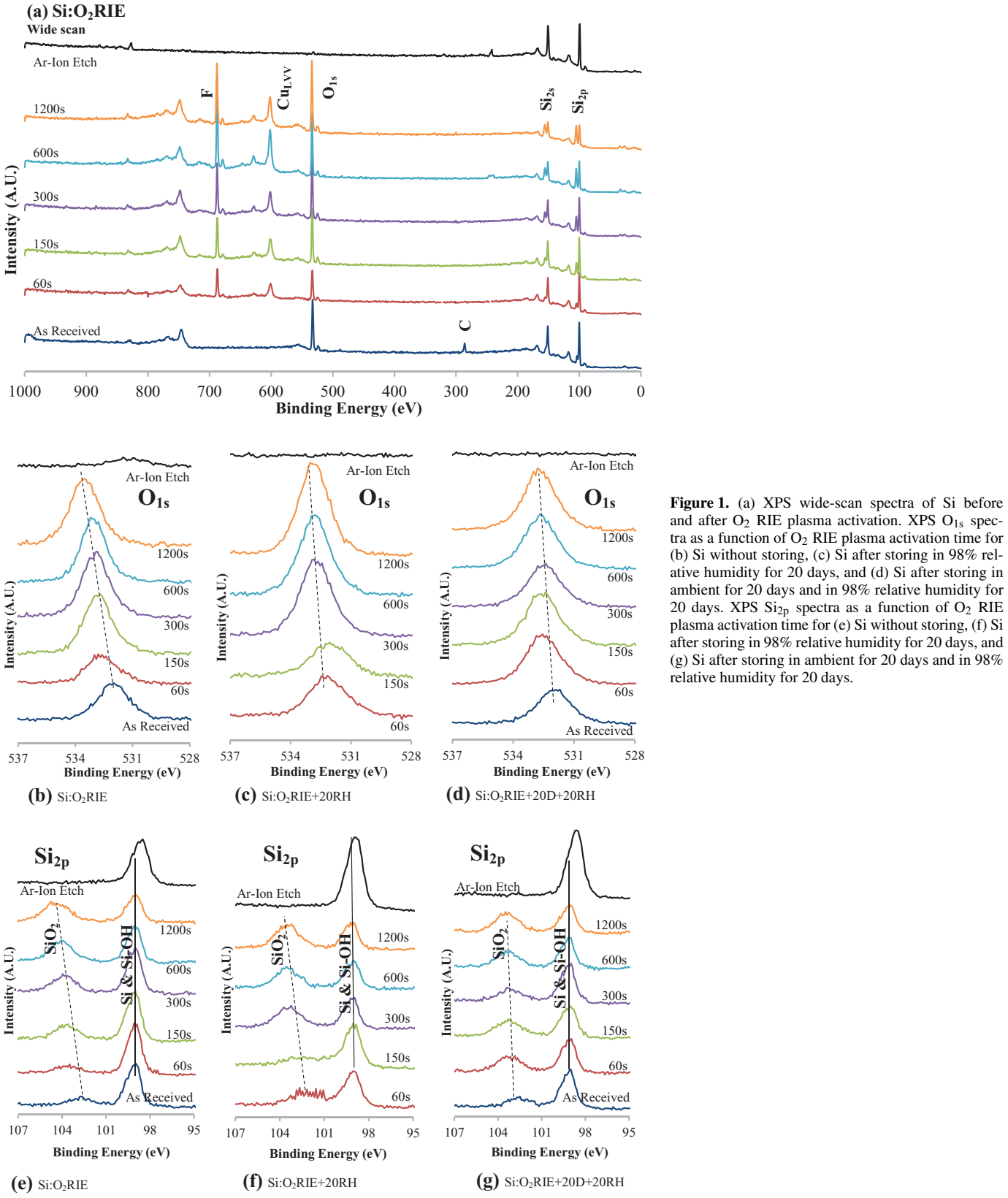

Figure 1. (a) XPS wide-scan spectra of Si before and after O_2 RIE plasma activation. XPS O_{1s} spectra as a function of O_2 RIE plasma activation time for (b) Si without storing, (c) Si after storing in 98% relative humidity for 20 days, and (d) Si after storing in ambient for 20 days and in 98% relative humidity for 20 days. XPS Si_{2p} spectra as a function of O_2 RIE plasma activation time for (e) Si without storing, (f) Si after storing in 98% relative humidity for 20 days, and (g) Si after storing in ambient for 20 days and in 98% relative humidity for 20 days.

The summarized amount of $Si(-O)_2$, $Si(-OH)_x$ and $Si(-O)_4$ components from the deconvolved O_{1s} spectra as a function of activation time storage conditions are shown in Figure 6. Figure 6a–6c corresponds to Figure 4b–4d, respectively. A decreasing trend of $Si(-O)_2$ and increasing trend of $Si(-OH)_x$ and $Si(-O)_4$ were observed with the increase of activation time.

Glass.— The wide-scan XPS spectra of glass surfaces before and after O_2 RIE plasma activation (i.e., Glass:O_2RIE) are shown in Figure 7a. Charge correction in this case was also done by shifting the position of the C peak binding energy at 284 eV. Before plasma activation, the as-received glass surface contained three major peaks: Si at ~106 eV, adventitious amorphous carbon at 284 eV and oxygen at 534 eV.[41]

Table II. Energy shift and change of FWHM of the deconvolved components of O_{1s} and Si_{2p} for Si at different plasma treatment and storage conditions. The energy shift and change of FWHM at any activation time are calculated with respect to the previous activation time/ condition. For example, the increase/decrease of energy shift at 60 s are calculated by comparing the components of the peak positions at 60s with respect to the components of the peaks positions for as received conditions. The upward and downward arrows indicate increase and decrease of energy and FWHM, respectively. "0" means no change.

			Shift of binding energy (eV)					Change of FWHM (eV)				
Condition	Element	Component	60s	150s	300s	600s	1200s	60s	150s	300s	600s	1200s
Si:O_2RIE	O_{1s}	Si-(OH)$_x$	↑0.5	↑0.1	0	↑0.5	↑0.4	↑0.2	↓0.1	↓0.2	↑0.1	↑0.1
		Si-(O)$_2$	↑0.7	↑0.1	↑0.1	↑0.4	↑0.2	↑0.1	↑0.1	↑0.1	↓0.1	0
		Si-(O)$_4$	↑0.6	↑0.3	↓0.2	↑0.1	↑0.8	↓0.2	↓0.1	↑0.2	0	↑0.1
	Si_{2p}	Si	0	0	0	0	0	↑0.2	↓0.1	0	↓0.1	0
		Si-(OH)$_x$	0	↑0.1	↓0.2	0	↑0.2	↓0.1	↑0.1	0	0	0
		Si-(O)$_2$	↑1.0	↑0.1	↑0.2	↑0.2	↑0.4	↑0.3	↓0.1	↓0.1	0	↑0.3
Si:O_2RIE+20RH	O_{1s}	Si-(OH)$_x$		0	↑0.8	↑0.2	0		↓0.2	0	↑0.1	↓0.1
		Si-(O)$_2$		↓0.2	↑0.6	↑0.2	0		↑0.1	↓0.1	0	0
		Si-(O)$_4$		0	↑0.3	↑0.4	↓0.1		0	0	0	0
	Si_{2p}	Si		0	0	0	0		↑0.1	↓0.1	0	0
		Si-(OH)$_x$		↑0.4	↓0.4	↓0.1	0		0	↓0.2	↑0.1	0
		Si-(O)$_2$		↑0.2	↑1.0	↑0.1	0		0	0	↓0.1	0
Si:O_2RIE+20D+20RH	O_{1s}	Si-(OH)$_x$	↑0.5	↑0.3	↓0.2	↑0.2	↓0.1	0	↑0.1	↓0.1	0	↓0.1
		Si-(O)$_2$	↑0.6	0	0	↑0.2	0	0	0	0	0	0
		Si-(O)$_4$	↑0.3	↓0.1	0	↑0.3	0	↓0.1	0	0	0	↓0.1
	Si_{2p}	Si	0	0	0	0	0	0	↑0.2	↓0.2	↑0.1	↓0.1
		Si-(OH)$_x$	0	↑0.1	↑0.1	0	↓0.1	0	0	0	0	0
		Si-(O)$_2$	↑0.7	0	↓0.1	↑0.2	↑0.1	↑0.1	0	↓0.1	0	0

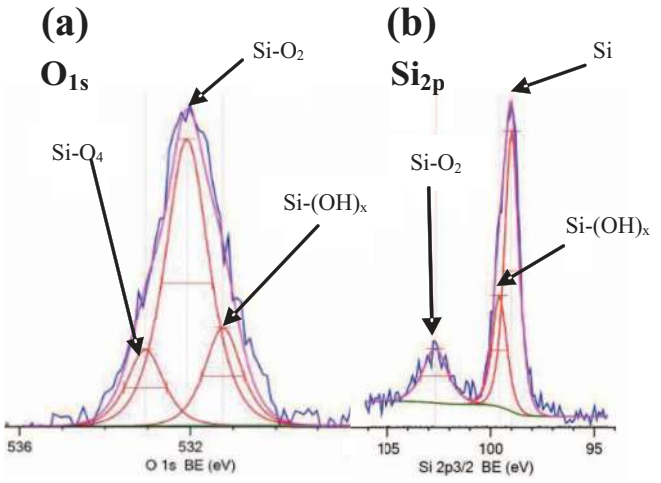

Figure 2. Deconvolved XPS spectra of (a) O_{1s} and (b) Si_{2p} for as-received Si.

After O_2 RIE plasma activation, additional peaks were observed at 270, 600, 690, 933 and 953 eV which are due to Na_{KLL}, Cu_{LVV}, F, $Cu_{2p3/2}$ and $Cu_{2p1/2}$ respectively.[41,46,47] Figure 7b, 7c and 7d show the high resolution XPS spectra of O_{1s}, Si_{2p} and Carbon and other peaks, respectively for Glass:O_2RIE. The solid line in Figure 7b shows the O_{1s} peak that appeared at 530.5 eV due to alkaline oxides. The silicon oxides peak (indicated by the dashed line in Figure 7b) shifted to higher binding energy with increased activation time.[30] In Figure 7c, the peak for the as received surface at ~106 eV was due to Si_{2p}.

Discussion

Silicon.— The presence of fluorine peaks in the wide-scan spectra of plasma-activated Si (Figure 1a) might be due to physisorbed or chemisorbed surface contaminants during hydrofluoric acid treatment for wafer cleaning.[47] The presence of Cu_{LVV} peak (Figure 1a) is due to the copper clamp used for holding the specimens during XPS acquisition. The significant positive binding energy shift and change of FWHM of Si-(OH)$_x$, Si-(O)$_2$, Si-(O)$_4$ components for Si:O_2RIE

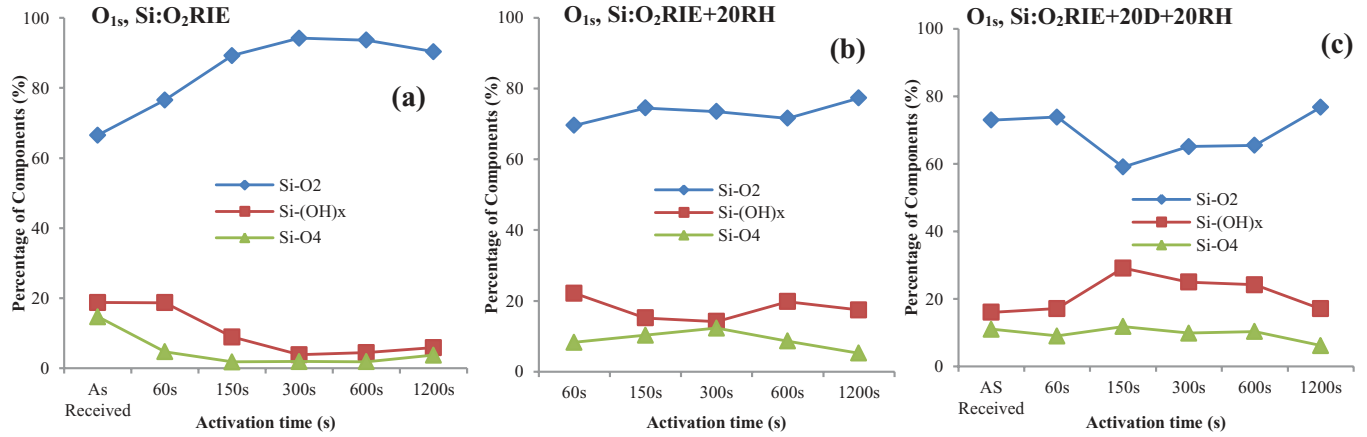

Figure 3. Percentage of Si-(O)$_2$, Si-(OH)$_x$ and Si-(O)$_4$ components in O_{1s} XPS spectra of (a) Si without storing, (b) Si after storing in 98% relative humidity for 20 days, and (c) Si after storing in ambient for 20 days and in 98% relative humidity for 20 days.

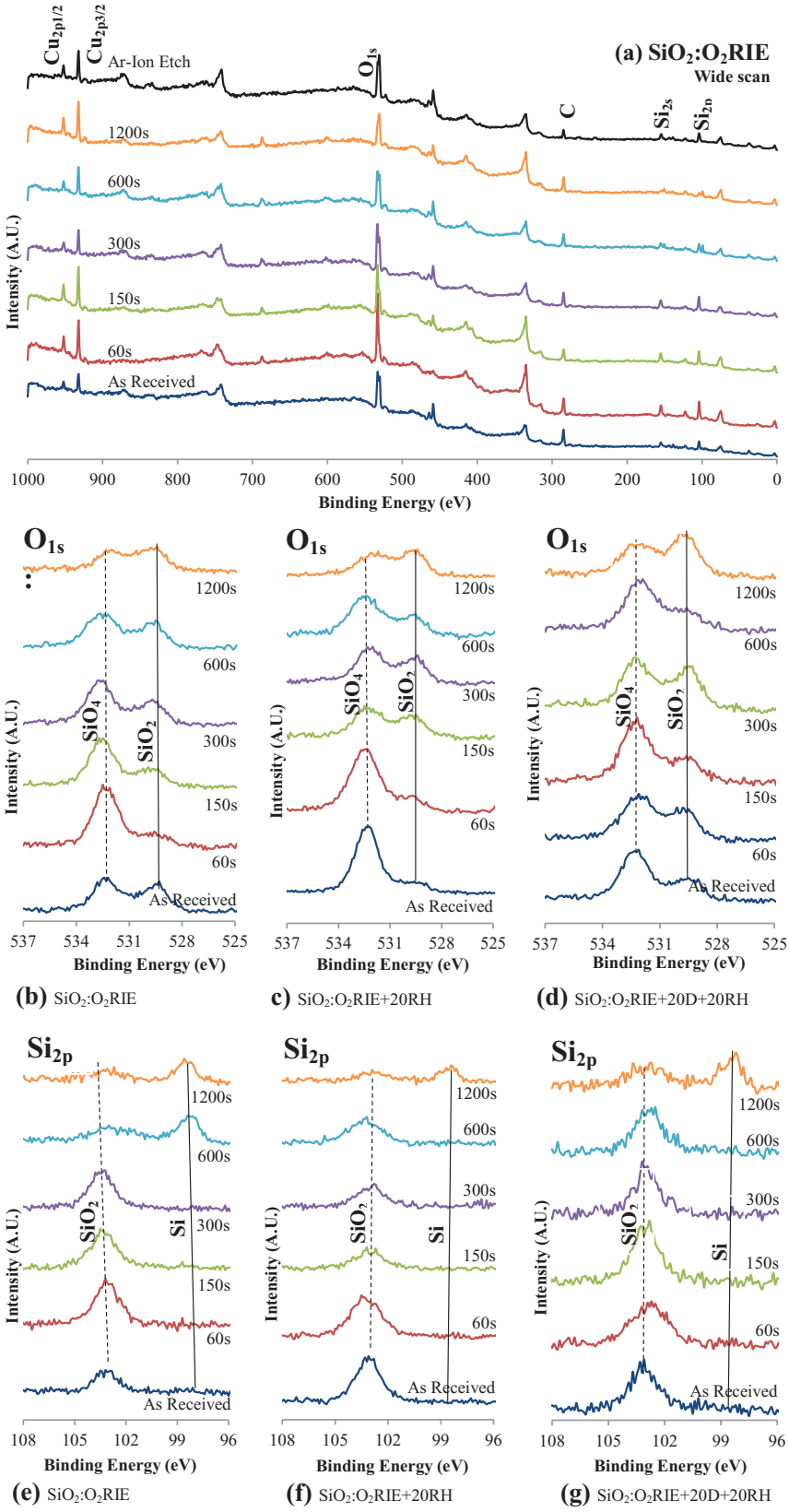

Figure 4. (a) XPS wide-scan spectra of SiO_2 before and after O_2 RIE plasma activation. XPS O_{1s} spectra as a function of O_2 RIE plasma activation time for (b) SiO_2 without storing, (c) SiO_2 after storing in 98% relative humidity for 20 days, and (d) SiO_2 after storing in ambient for 20 days and in 98% relative humidity for 20 days. XPS Si_{2p} spectra as a function of O_2 RIE plasma activation time for (e) SiO_2 without storing, (f) SiO_2 after storing in 98% relative humidity for 20 days, and (g) SiO_2 after storing in ambient for 20 days and in 98% relative humidity for 20 days.

(Table II) is due to the O_2 RIE oxidation of the surface. Also, the considerable energy shift of $Si(-O)_2$ and $Si(-OH)_x$ in the case of $Si:O_2RIE+20RH$ indicates the overlapping of the O_2 RIE oxidation (i.e., $Si(-O)_2$) of the surface by the water molecules from humidity storage (i.e., $Si(-OH)_x$). And the considerable positive binding energy shift of only $Si(-OH)_x$ component for $Si:O_2RIE+20D+20RH$ suggests a significant Si-OH layer covering the treated Si substrate.

The shifts in the binding energies (Table II) also show the dependence of the chemical changes of the surface functional groups resulting from reactions due to the O_2 RIE oxide film, ambient

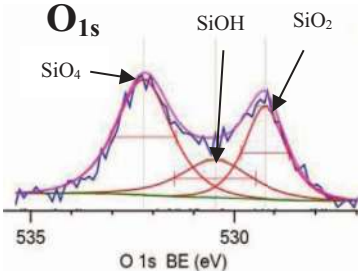

Figure 5. Deconvolved XPS spectra of O_{1s} for as-received Si.

conditions and humidity.[25] In general, oxidation of atoms shifts their binding energy.[26] Higher oxidation results in a higher shift in the binding energy.[41] This indicates that increased activation time using O_2 RIE plasma shifts Si(-OH)$_x$, Si(-O)$_2$, Si(-O)$_4$ component peaks into higher binding energies. The high surface reactivity for Si:O_2RIE may also be attributed to energy shift of Si(-O)$_2$.[40] For, Si:O_2RIE+20RH and Si:O_2RIE+20D+20RH, the insignificant shift in binding energy of Si(-O)$_2$ and significant shift to that of Si(-OH)$_x$ may be attributed to the introduction of humidity and reduction in surface reactivity. The 'Ar-ion Etch' curves in Figure 1 also supports the conclusion in Refs. 26,41 that oxidation plays a major role in shifting the binding energy. The etched surface shows Si peak at a lower binding energy than that of the as-received surface.

The variation of Si(-O)$_2$, Si(-OH)$_x$ and Si(-O)$_4$ as a function of activation time and storage in ambient humidity and/or controlled humidity (Figure 3) may be explained by the plasma-induced changes in surface roughness and crystal-orientation dependent oxidation. The oxidation rate is defined as the rate of reaction between water molecules and silicon bonds at the silica-silicon interface.[48] The Si surface in our experiment has (100) crystal orientation. The number of available bonds per cm^2 to react with water (known as N) is the smallest in (100) crystal orientation. As the roughness of the Si surface increases, other crystal orientations such as (110), (111) and (311) are more exposed to the water molecules derived from the ambient and humidity chamber. These orientations have higher value of N as compared to (100) orientation resulting in larger oxidation rates.[48]

With the increasing activation time up to 150 s, the surface roughness of Si surface is not increased significantly (i.e., ~0.25 nm at 150 s for Si:O_2RIE+20D+20RH), as compared to the higher activation times (e.g., ~2.5 nm at 1200 s for Si:O_2RIE+20D+20RH).[40] Thus, the percentage of Si(-O)$_2$ component decreases until 150 s in Figure 3c due to lower surface roughness. This lower surfaces roughness does not allow the exposing of other crystal orientations. On the other hand, the Si(-O)$_2$ increases from 300 to 1200 s due to high surface roughness. The high surface roughness dominantly oxidizes due to the exposure of crystal orientations other than (100).

The increase of Si(-OH)$_x$ until 150 s and then its decrease (Figure 3c) is also correlated with the surface roughness and oxidation. Due to lower surface roughness until 150 s, the accumulated water is higher compared to that of the higher surface roughness. Here the total surface area plays a dominant role in increasing the Si(-OH)$_x$ on the surface. With higher surface roughness, the total surface area increases significantly which results in decreased Si(-OH)$_x$, as shown in the activation time from 300 to 1200 s. However, these explanations that assume a crystal orientation dependent oxidation may be incorrect if there is decreased oxidation rate at higher surface roughness due to exposure of least reactive crystal planes (e.g., (111)).[49]

The plasma-induced Si(-O)$_2$ and Si(-OH)$_x$ increase the surface reactivity and hydrophilicity that control the direct bonding of Si based substrates.[40] The higher amount of Si(-OH)$_x$ below 300 s (Figure 3a) activation time for Si:O_2RIE control the sorption on the surface that directly involves in the hydrophilic wafer bonding.[50] Also, the Si(-O)$_4$ is required for the absorption of voids. These results are consistent with the summary table (Table III) of surface properties and bondability in Refs. 34,41,51,52. The humidity and ambient induced Si-(OH)$_x$ also plays a significant role in enhanced adhesion for good bondability with low temperature heating (below 300°C).[50]

Silicon dioxide.— The Cu peaks in SiO_2:O_2RIE is due to the copper clamp in the specimen holder. As compared to Si and glass, SiO_2 has stronger Cu peaks. This is due to smaller specimen size of SiO_2 resulting in the incorporation of Cu clamps into the XPS acquisition area. In contrast to Si (Figure 1), no considerable binding energy shift and change of FWHM was observed in the case of SiO_2 (Figure 4). This could be due to the negligible surface charging caused by the oxygen RIE plasma activation as compared to that of the Si surface. This behavior also relates to the minor variation in the contact angle of SiO_2.[40]

The higher amount of Si(-OH)$_x$ in SiO_2:O_2RIE+20RH and SiO_2:O_2RIE+20D+20RH than that of SiO_2:O_2RIE (Figure 6) attributed to its affinity with water molecule from the ambient humidity and controlled humidity storage resulting in higher hydrophilicity. The presence of Si(-OH)$_x$ after plasma-activation and its increase after humidity and ambient treatment is good for hydrophilic wafer bonding at low temperature. The surfaces of wafers are mostly hydrophilic immediately after exposure to oxygen plasma, and the hydrophilicity decreases with increasing storage time. However, in our case, contact angle measurements of SiO_2:O_2RIE+20D+20RH showed increased

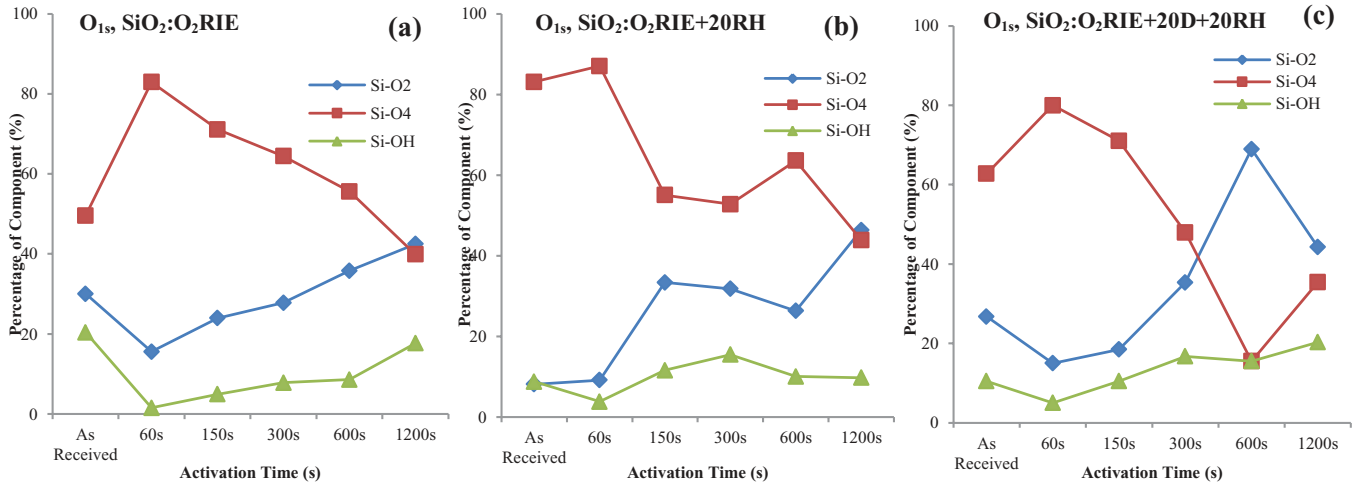

Figure 6. Percentage of Si-(O)$_2$, Si-(O)$_4$ and Si-(OH)$_x$ components in O_{1s} XPS spectra of (a) SiO_2 without storing, (b) SiO_2 after storing in 98% relative humidity for 20 days, and (c) SiO_2 after storing in ambient for 20 days and in 98% relative humidity for 20 days.

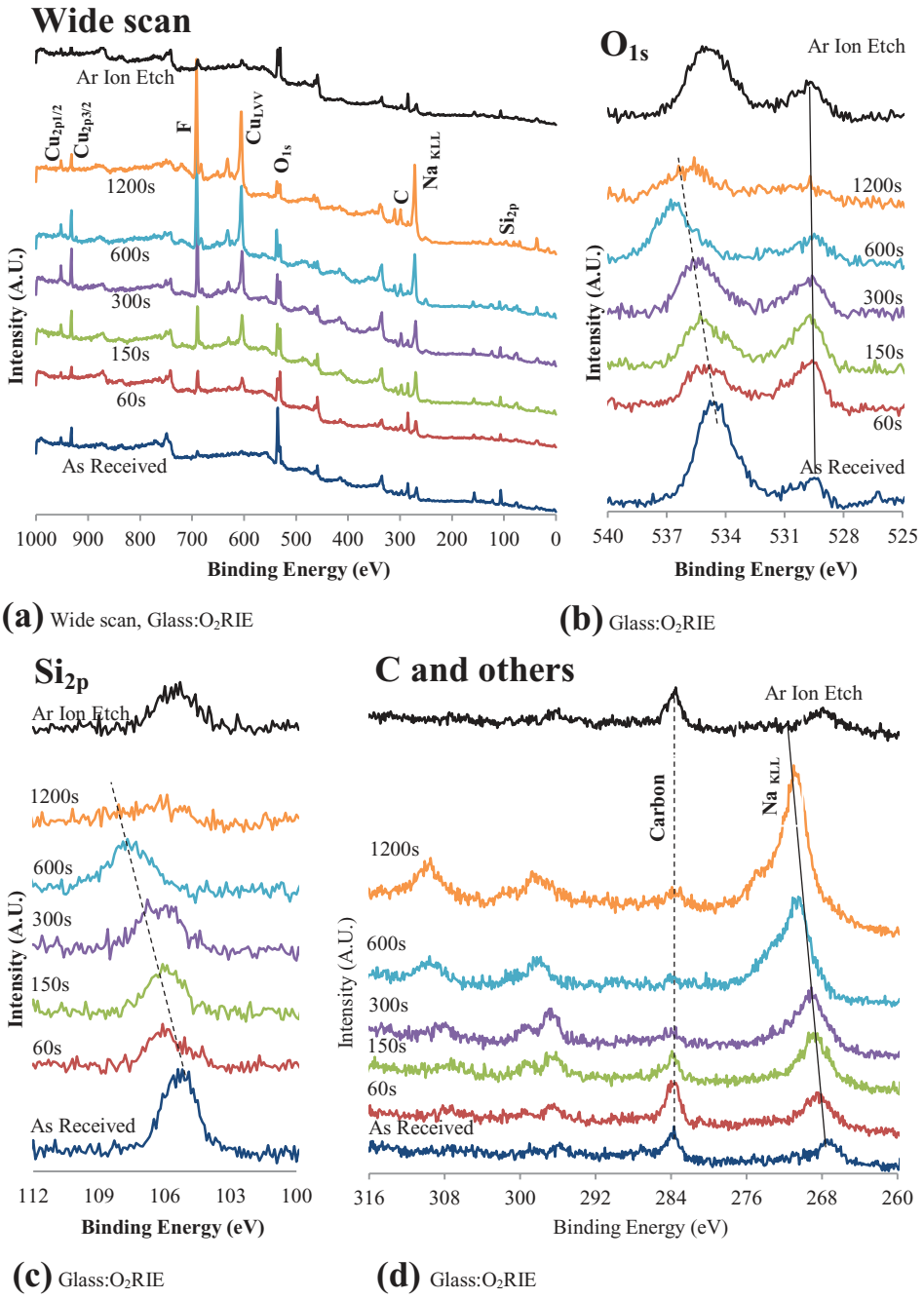

Figure 7. (a) XPS wide-scan spectra of glass. (b) XPS O_{1s} spectra of glass after O_2 RIE plasma activation (c) XPS Si_{2p} spectra of glass after O_2 RIE plasma activation (d) XPS C_{1s} spectra of glass after O_2 RIE plasma activation.

Table III. Evolution of Surface properties with the increase of oxygen plasma activation times at different storage conditions.

	Change in surface chemical properties with the increase of activation times (60, 150, 300, and 600 s) under different storage conditions			
Surface Treatment	Shift in the Binding Energy	Amount of $Si(-O)_2$	Amount of $Si(-OH)_x$	Bondability
$Si:O_2RIE$	High	Increase	High until 150 s activation time	Better at lower activation time[40,50,51]
$Si:O_2RIE+20RH$	Low	Increase	Increase	Good at lower activation
$Si:O_2RIE+20D+20RH$	Low	Increase	Increase	Good at lower activation
$SiO_2:O_2RIE$	Negligible	Decrease	Increase	Better at lower activation time
$SiO_2:O_2RIE+20RH$	Negligible	Decrease	Increase	Better at lower activation time
$SiO_2:O_2RIE+20D+20RH$	Negligible	Decrease	Increase	Good at lower activation
$Glass:O_2RIE$	Only for Si-based oxides	–	–	Better at low activation time

hydrophilicity, in agreement with the results in.[40] The amount of $Si(-O)_2$ and $Si(-OH)_x$ might have influence on the reduction of hardness of SiO_2 with the increase of O_2 RIE activation time.[40]

Glass.— The presence of O_{1s} peak at 530.5 eV in Figure 7b is related to oxides of alkaline elements other than Si. This is because the peak does not shift with the increase of O_2 RIE activation times.[30] While the peak grows in amplitude after 60 s and 150 s, its growth weakens with increased treatment time. Similarly, the intensity of the Carbon (∼284 eV, Fig. 7d) peak increases at 60 s and then again decreases until 1200 s. In fact, while the alkaline oxide peak completely disappears at 1200 s, the C peak still remains. The remaining C at 1200 s may be caused by prolonged irradiation to the glass. Also, the increase of Na_{KLL} peak is evident which may be indicative of the presence of alkaline oxides. Therefore the identical behavior both for Carbon (∼284 eV) and O_{1s} (530.5 eV) peaks supports the presence of alkaline oxides.

The study of Pyrex glass using quantum cascade laser absorption spectroscopy[53] showed that oxygen plasma treatment of Pyrex glass materials resulted in a highly oxygen saturated surface. In a study of anodic bonding of GaAs and Pyrex glass[54] using sequential plasma activation (i.e., O_2 RIE plasma and N_2 microwave plasma), it was found that the low-frequency Raman peaks were due to alkaline–oxygen–alkaline stretching, Si–O–Si networks and aluminate networks (Al–O/Al–O–B). After plasma activation, the intensity of these peaks was enhanced with their shapes unchanged. These results also support the presence of silicon oxides and alkaline oxides. At 1200 s, the silicon oxides peak (∼535 eV) becomes weak, similar to the peak at 530.5 eV (Figure 7b). The prolonged activation results in an opaque surface due to severe damage. The damage increased the surface roughness ∼100 times compared to that of the as-received surface.[40] The high surface roughness may be attributed to the oxidation of the alkaline elements of the glass during prolonged O_2 RIE activation. Thus, lower activation time is suitable for better bondability in glass-based wafer bonding.[40]

The Si_{2p} peak at 106 eV in Figure 7c broadens after O_2 RIE activation at different time and shifts to higher energy due to the oxidation of Si. The deconvolution of the broadened peaks using mixed Gaussian-Lorentzian curve fitting revealed two peaks consisting of silicon-dioxide and sub-oxides.[55] In fact, at 1200 s, the silicon-dioxide and sub-oxides peaks are almost disappeared. After Ar ion etching of the as-received specimen, Si_{2p} peak is appeared at binding energy lower than that of O_2 RIE plasma treated surface but identical to that of as-received surface. Therefore, the comparison among the as-received, O_2 RIE treated and Ar ion etched surface indicate that the O_2 RIE results in silicon-dioxide and sub-oxides on glass. A comparison in the change of the surface chemical properties of the specimens with increase in activation time is summarized in Table III.

Conclusions

X-ray photoelectron spectroscopy (XPS) of silicon (Si), silicon dioxide (SiO_2) and glass surfaces was studied after treating in oxygen reactive ion etching plasma followed by exposure in humidity and/or ambient. Before plasma activation, wide-scan XPS of Si and SiO_2 showed Si_{2p}, Si_{2s}, C and O_{1s} peaks, and glass showed the same peaks plus an additional peak of sodium. The O_2 RIE plasma showed increase of O_{1s} peak intensity with increased plasma activation time. An unwanted peak of fluorine was observed only in Si and glass. This fluorine is due to physisorbed or chemisorbed contaminant from the wafer cleaning using hydrofluoric acid.

High resolution XPS spectra of Si before and after O_2 RIE plasma treatment showed that $Si(-O)_2$ was shifted to higher binding energy, which could be correlated with the high surface reactivity of Si. After storage of the activated Si wafers in controlled humidity, significant overlap of silicon oxide (i.e., $Si(-O)_2$) and silanol groups (i.e., $Si(-OH)_x$) were observed. Also, a considerable coverage of silanol groups was evident after storage in the ambient humidity and controlled humidity. Increased coverage of silanol group is indicative of the interaction of water molecules with the Si surfaces. The variation of $Si(-O)_2$ and $Si(-OH)_x$ components at different activation times was due to crystal-orientation dependent surface roughness and oxidation rate, although the least reactive crystal planes (e.g., (111)) might have decreased oxidation. However, the increased amount of $Si(-OH)_x$ at activation times below 300 s seem preferable for bonding with low temperature heating.

Unlike Si, the high resolution XPS of SiO_2 showed insignificant shift in binding energy which is attributed to its high insulating property. However, presence of $Si(-O)_2$ due to oxygen plasma oxidation and increase of $Si(-OH)_x$ due to humidity storage were observed. Oxygen plasma activation of glass showed oxide peaks due to Si and other alkalines. Also, the silicon oxides and sub-oxides appeared to be due to plasma oxidation. Prolonged activation caused opaque glass surface and high surface roughness due to damage. This high surface reactivity of Si, SiO_2 and glass wafers at lower activation times, and increased amount of $Si(-OH)_x$ after humidity storage greatly influence their hydrophilic direct wafer bonding.

Acknowledgments

This research is supported by discovery grants from the Natural Science and Engineering Research Council (NSERC) of Canada, an infrastructure grant from the Canada Foundation for Innovation (CFI) and an Ontario Research Fund for Research Excellence Funding grant. The authors gratefully acknowledge Fangfang Zhang for her help with the Hybrid Plasma Bonder. Also, the authors acknowledge to Professor Peter Kruse of Chemistry Department at McMaster University for his comments on the XPS results.

References

1. Y. Huang, A. Sai Sarathi Vasan, R. Doraiswami, M. Osterman, and M. Pecht, *IEEE Trans. Device Mater. Reliab.*, **12**, 482 (2012).
2. A. G. Darrin and R. Osiander, *MEMS Materials and Processes Handbook*, p. 879, Springer, Boston (2011).
3. M. W. Shinwari, M. J. Deen, and D. Landheer, *Microelectron. Reliab.*, **47**, 2025 (2007).
4. M. M. R. Howlader, P. R. Selvaganapathy, M. J. Deen, and T. Suga, *IEEE J. Sel. Top. Quantum Electron.*, **17**, 689 (2011).
5. M. W. Shinwari, D. Zhitomirsky, I. A. Deen, P. R. Selvaganapathy, M. J. Deen, and D. Landheer, *Sensors*, **10**, 1679 (2010).
6. G. Kräuter, A. Schumacher, and U. Gösele, *Sens. Actuators, A*, **70**, 271 (1998).
7. H. Takagi, R. Maeda, T. R. Chung, and T. Suga, *Sens. Actuators, A*, **70**, 164 (1998).
8. J. Wei, S. M. L. Nai, C. K. Wong, and L. C. Lee, *Thin Solid Films*, **462–463**, 487 (2004).
9. T. Suni, K. Henttinen, a. Lipsanen, J. Dekker, H. Luoto, and M. Kulawski, *J. Electrochem. Soc.*, **153**, G78 (2006).
10. F. Zhang, M. Kibria, K. Cormier, and M. M. R. Howlader, *ECS Trans.*, **33**, 329 (2010).
11. R. H. Esser, K. D. Hobart, and F. J. Kub, *J. Electrochem. Soc.*, **150**, G228 (2003).
12. M. K. Weldon and J. Vac. *Sci. Technol. B Microelectron. Nanom. Struct.*, **14**, 3095 (1996).
13. R. Joyce, K. Singh, H. Sharma, S. Varghese, and J. Akhtar, *Microsyst. Technol.*, **19**(6) (2013).
14. A. Sanz-Velasco, P. Amirfeiz, S. Bengtsson, and C. Colinge, *J. Electrochem. Soc.*, **150**, G155 (2003).
15. X. Ma, C. Chen, W. Liu, X. Liu, X. Du, Z. Song, and C. Lin, *J. Electrochem. Soc.*, **156**, H307 (2009).
16. M. M. R. Howlader, F. Zhang, and M. G. Kibria, *J. Micromech. Microeng.*, **20**, 065012 (2010).
17. T. Suni, K. Henttinen, I. Suni, and J. Mäkinen, *J. Electrochem. Soc.*, **149**, G348 (2002).
18. Q.-Y. Tong, *J. Electrochem. Soc.*, **144**, 384 (1997).
19. T. L. Barr, *Appl. Surf. Sci.*, **15**, 1 (1983).
20. K. Y. Byun, P. Fleming, N. Bennett, F. Gity, P. McNally, M. Morris, I. Ferain, and C. Colinge, *J. Appl. Phys.*, **109**, 123529 (2011).
21. S. N. Farrens, J. R. Dekker, K. Smith, K. Jason, and B. E. Roberds, *J. Electrochem. Soc.*, **142**, 3949 (1995).
22. V. A. Labunov and P. V. Protasevich, *Nucl. Instruments Methods Phys. Res.*, **B39**, 466 (1989).
23. S. Vepiek, Z. Iqbal, H. R. Oswald, and A. P. Webb, *J. Phys. C Solid State Phys.*, **14**, 295 (1981).
24. K. T. Sung, *J. Vac. Sci. Technol., B*, **10**, 2211 (1992).
25. K. J. Trevino, J. C. Shearer, B. D. Tompkins, and E. R. Fisher, *Plasma Process. Polym.*, **8**, 951 (2011).

26. T. Hattori, H. Yamagishi, N. Koike, K. Imai, and K. Yamabe, *Appl. Surf. Sci.*, **41**, 416 (1989).
27. S. A. Nelson, H. D. Hailen, and R. A. Buhrman, *J. Appl. Phys.*, **63**, 5027 (1988).
28. A. Mekki, D. Holland, C. F. McConville, and M. Salim, *J. Non. Cryst. Solids*, **208**, 267 (1996).
29. Y. C. Araujo, P. G. Toledo, V. Leon, and H. Y. Gonzalez, *J. Colloid Interface Sci.*, **176**, 485 (1995).
30. J. Park and A. Tseng, *Proceedings of 2004 JUSFA*, pp. 1–7, 2004.
31. A. A. Tseng, J.-S. Park, G. P. Vakanas, H. Wu, M. Raudensky, and T. P. Chen, *Microsyst. Technol.*, **13**, 49 (2006).
32. T. Miura, Y. Benino, R. Sato, and T. Komatsu, *J. Eur. Ceram. Soc.*, **23**, 409 (2003).
33. S. Bengtsson and P. Amirfeiz, *J. Electron. Mat.*, **29**, 909 (2000).
34. M. M. R. Howlader, G. Kagami, S. H. Lee, J. G. Wang, M. J. Kim, and A. Yamauchi, *J. Microelectromech. Syst.*, **19**, 840 (2010).
35. M. G. Kibria, F. Zhang, T. H. Lee, M. J. Kim, and M. M. R. Howlader, *Nanotechnology*, **21**, 134011 (2010).
36. M. M. R. Howlader, S. Suehara, and T. Suga, *Sens. Actuators, A*, **127**, 31 (2006).
37. S. Luo and C. P. Wong, *IEEE Trans. Components Packag. Technol.*, **28**, 88 (2005).
38. H. Khlyap, V. Laptev, L. Pankiv, and V. Tsmots, *Crystalline Silicon - Properties and Uses*, p. 43, InTech, Rijeka, Croatia (2011).
39. M. M. R. Howlader, M. G. Kibria, F. Zhang, and M. J. Kim, *Talanta*, **82**, 508 (2010).
40. A. U. Alam, M. M. R. Howlader, and M. J. Deen, *Unpublished Manuscript*, October, 2013.
41. JEOL, "Handbook of X-ray Photoelectron Spectroscopy", pp. 10-20, Japan, 1991.
42. D.-I. Kim, K.-H. Kim, and H.-S. Ahn, *Int. J. Precis. Eng. Manuf.*, **11**, 741 (2010).
43. M. Grundner and H. Jacob, *Appl. Phys., A*, **39**, 73 (1986).
44. S. P. Kobeleva, T. G. Sergeeva, B. M. Leiferov, and a. L. Ivanova, *Phys. A Stat. Mech. its Appl.*, **241**, 398 (1997).
45. A. Verdaguer, C. Weis, G. Oncins, G. Ketteler, H. Bluhm, and M. Salmeron, *Langmuir*, **23**, 9699 (2007).
46. F. Leisenberger, R. Duschek, R. Czaputa, F. P. Netzer, G. Beamson, and J. a. D. Matthew, *Appl. Surf. Sci.*, **108**, 273 (1997).
47. W. Kern, *J. Electrochem. Soc.*, **137**, 1887 (1990).
48. J. R. Ligenza, *J. Phys. Chem.*, **65**, 2011 (1961).
49. R. E. Oosterbroek, J. W. Berenschot, H. V. Jansen, A. J. Nijdam, G. Pandraud, A. van den Berg, and M. C. Elwenspoek, *J. Microelectromech. Syst.*, **9**, 390 (2000).
50. T. Plach, K. Hingerl, S. Tollabimazraehno, G. Hesser, V. Dragoi, and M. Wimplinger, *J. Appl. Phys.*, **113**, 094905 (2013).
51. M. M. R. Howlader, T. Suga, H. Itoh, T. H. Lee, and M. J. Kim, *J. Electrochem. Soc.*, **156**, H846 (2009).
52. M. M. R. Howlader, F. Zhang, and M. J. Kim, *J. Microelectromech. Syst.*, **20**, 17 (2011).
53. O. Guaitella, M. Hübner, S. Welzel, D. Marinov, J. Röpcke, and a. Rousseau, *Plasma Sources Sci. Technol.*, **19**, 045026 (2010).
54. M. M. R. Howlader, F. Zhang, and M. Jamal Deen, *Nanotechnology*, **24**, 315301 (2013).
55. J.-W. He, X. Xu, J. S. Corneille, and D. W. Goodman, *Surf. Sci.*, **279**, 119 (1992).